Supporting Information

The effect of activation time on water sorption behavior of nitrogen-doped, physically activated, monolithic carbon for adsorption cooling

Lukas Huber[a], Stefanie Beatrice Hauser[a], Eric Brendlé[b], Patrick Ruch[c], Jens Ammann[c], Roland Hauert[d], Remo N. Widmer[e], Christopher J. Ubert[a], Santhosh Kumar Matam[e], Songhak Yoon[e], Yucheng Zhang[f], Matthias M. Koebel[a,*]

[a]*Empa, Swiss Federal Laboratories for Materials Science and Technology, Laboratory for Building Energy Materials and Components, Überlandstrasse 129, CH-8600 Dübendorf, Switzerland*

[b]*Adscientis, 1 rue Alfred Kastler, 68310 Wittelsheim, France*

[c]*IBM Research GmbH, Säumerstrasse 4, CH-8803 Rüschlikon, Switzerland*

[d]*Empa, Swiss Federal Laboratories for Materials Science and Technology, Laboratory for Joining Technologies & Corrosion, Überlandstrasse 129, CH-8600 Dübendorf, Switzerland*

[e]*Empa, Swiss Federal Laboratories for Materials Science and Technology, Materials for Energy Conversion Laboratory, Überlandstrasse 129, CH-8600 Dübendorf, Switzerland*

[f]*Empa, Swiss Federal Laboratories for Materials Science and Technology, Electron Microscopy Center, Überlandstrasse 129, CH-8600 Dübendorf, Switzerland*

** Corresponding author. Tel: +41 58 765 4780. E-mail: Matthias.Koebel@empa.ch*

1. Scanning electron microscopy (SEM)

Figure S1 shows the SEM micrographs for the dried RUF resin, the pyrolyzed as well as the activated carbon. It was observed that the pyrolyzed as well as the activated carbon consists of irregularly polyhedral particles with the size from hundreds of nanometers to a few micrometers.

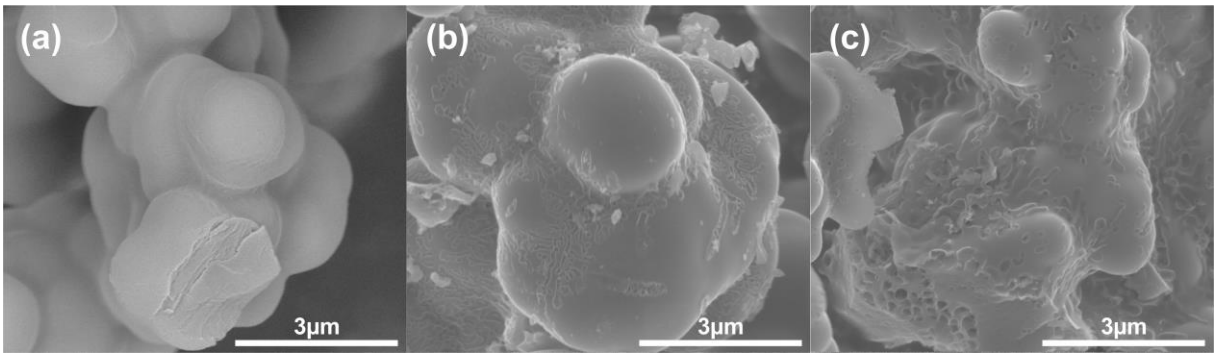

Figure S1. Secondary electron SEM images of the (a) RUF resin, (b) RUF-p900, and (c) RUF-p900-CO2-3h

2. Transmission electron microscopy (TEM)

The HRTEM images, in Figure S2, of the sample RUF-p900 reveal a disordered mesoporous network.

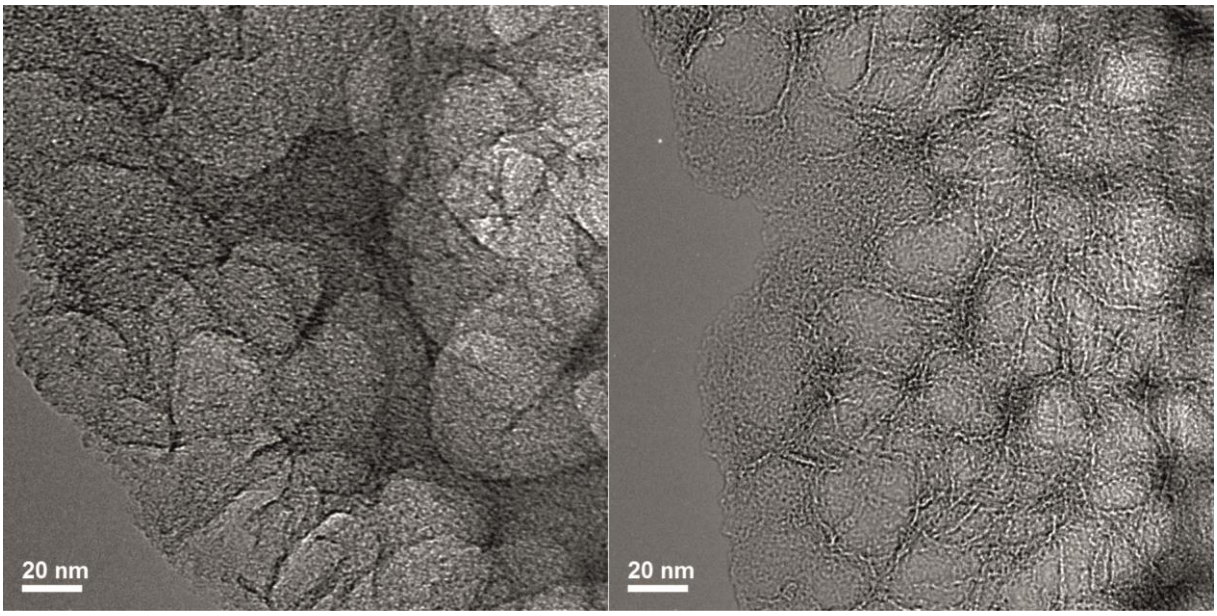

Figure S2. HRTEM micrographs of the sample RUF-p900

3. Raman spectroscopy

Samples were cut with a diamond saw into cylinders with a diameter of 12 mm and a height of 4 mm. After washing in acetone in an ultrasonic bath, the samples were dried in an oven at 50°C overnight.

All Raman spectra were obtained in air at room temperature on a Renishaw 2000 spectrometer equipped with holographic notch filters for elastic scattering and a CCD array detector. The data was accumulated with a WiRE software while the samples were excited with a HeNe laser (632.816 nm). A 20x objective was used to focus the laser onto the sample. The instrument was calibrated with a Si single crystal (Raman band at ~520 cm^{-1}). The spectra were recorded with an exposure time of 30 s and accumulation number of 5.

The Raman spectra of the RUF-derived carbons pyrolyzed and activated in CO_2 for different times are shown in Figure S3. Two wide bands are present at approximately 1360 cm^{-1} and 1580 cm^{-1}. The peak located at 1357 cm^{-1} (D-mode) is owed to a disordered structure in the carbons, whereas the peak close to 1580 cm^{-1} (G-mode) is due to the graphitic structure. With prolonged activation time, no significant change in the Raman spectra can be observed. For that reason, it can be concluded that there is no graphitization or pronounced improvement of ordering occurring for these samples, which is in agreement with the XRD results.

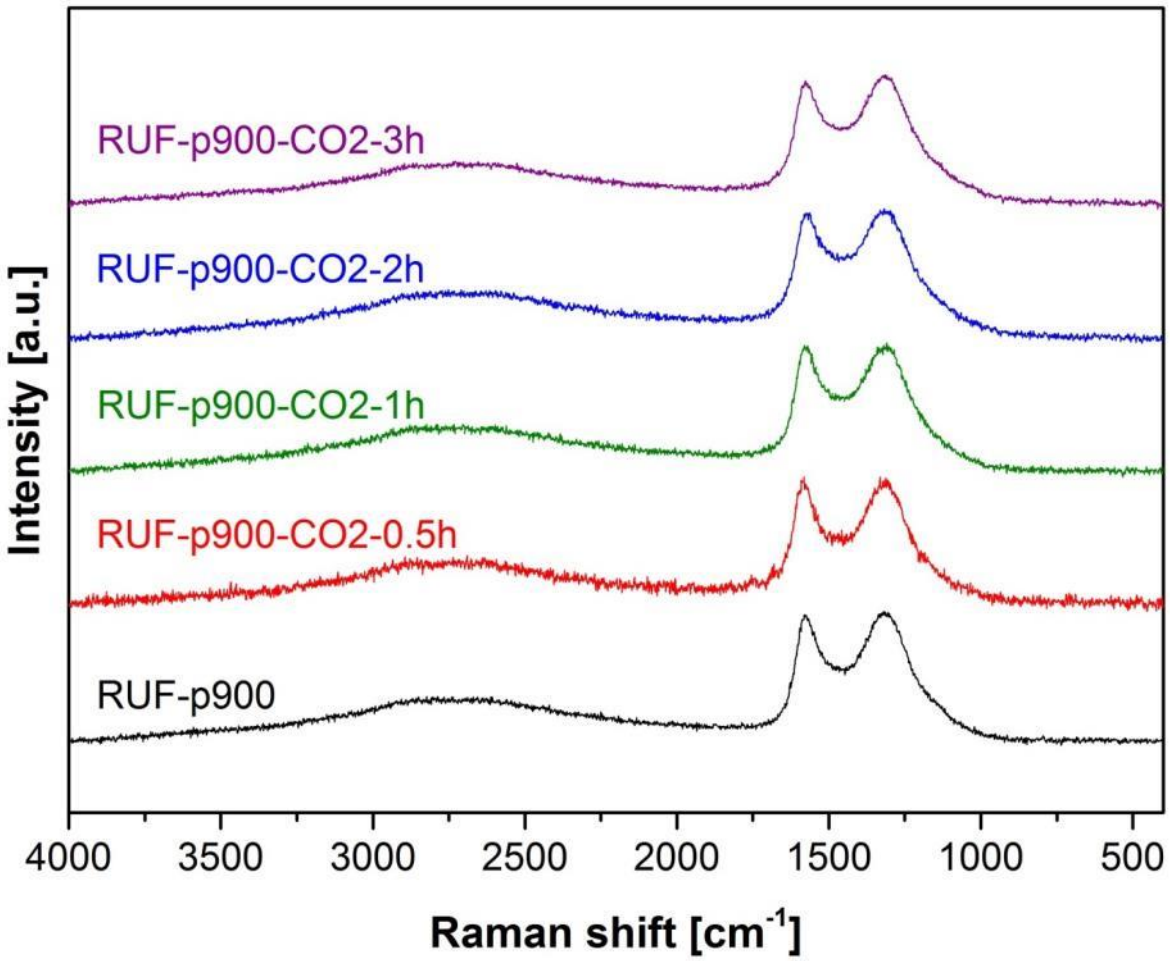

Figure S3. Raman spectra of the pyrolyzed as well as CO_2-activated carbons

4. X-ray photoelectron spectroscopy (XPS)

The N 1*s* spectra can be split into four different chemical states, namely pyridinic-type nitrogen (N-6), pyrrolic and/or pyridine-type nitrogen (N-5), quaternary nitrogen (N-Q), and pyridine nitrogen-oxide (N-X) with the relative peak distances fixed according to the values reported by Pels *et al.* [1]. Table S1 lists the relative contribution of each moiety. The full width at half maximum (FWHM) was fixed to be ≤ 2.2 eV. The average resulting peak positions were within ± 0.4 eV compared to the average reference values reported in literature [1,2].

No significant change of the relative composition of the four different states can be observed with prolonged activation times in CO_2.

Table S1. Binding energies and relative surface concentration of nitrogen species obtained by fitting the N 1*s* core level XPS spectra

Sample	N-6			N-5			N-Q			N-X		
	B.E. [eV]	FWHM	%	B.E. [eV]	FWHM	%	B.E. [eV]	FWHM	%	B.E. [eV]	FWHM	%
RUF-p900	398.51	1.96	38.58	400.11	1.06	4.17	401.01	1.53	40.43	402.81	2.2	16.82
RUF-p900-CO2-0.5h	398.38	1.46	25.91	399.98	1.33	12.70	400.88	1.94	46.78	402.68	2.2	14.61
RUF-p900-CO2-1h	398.49	1.91	36.79	400.09	1.04	9.38	400.99	1.52	38.35	402.79	2.2	15.48
RUF-p900-CO2-2h	398.83	2.2	42.98	400.43	1.39	20.55	401.33	1.5	23.15	403.13	2.2	13.31
RUF-p900-CO2-3h	398.83	2.2	40.30	400.43	1.23	19.28	401.33	1.55	27.25	403.13	2.2	13.16

5. Pore size distribution

BJH pore size distribution was determined from the desorption branch of the isotherm using the Barrett–Joyner–Halender (BJH) model [3] (Figure S4).

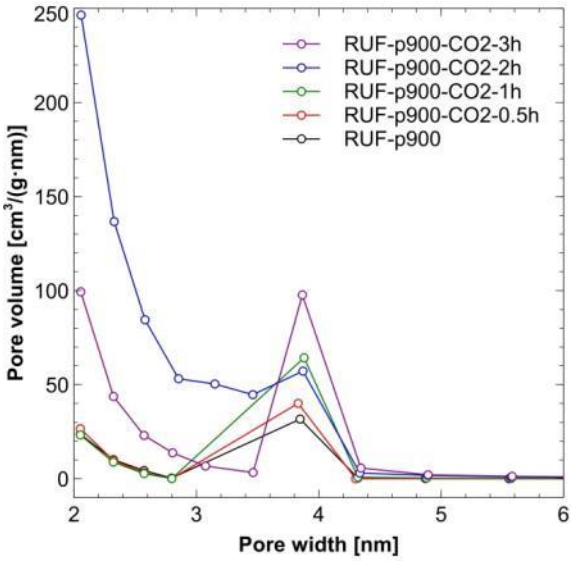

Figure S4. BJH poresize distribution of the pyrolyzed as well as activated carbons

6. Total pore volume

Various studies [4–6] have shown that, at saturation, the liquid volume of different adsorbates, when measured on porous adsorbents, is essentially constant and is independent of the adsorptive. The constancy of the adsorbed liquid volume at saturation is known as the Gurvich rule [7].

The pore volume, V_p, is given by

$$V_p = \frac{W_a}{\rho_l}$$

Where W_a is the adsorbed amount of water (in grams) and ρ_l the liquid density. A comparison of the pore volume calculated by the Gurvich rule and the pore volume calculated by nitrogen sorption at P/P_0=0.98 is shown in Table S2.

Table S2. Comparison of total pore volume by Gurvich with the pore volume by nitrogen sorption

Sample	Total pore volume by Gurvich [cm^3/g]	Pore volume by nitrogen sorption [cm^3/g]	Bulk liquid density of water [g/cm^3]
RUF-p900	0.147	0.261	0.56
RUF-p900-CO2-0.5h	0.232	0.273	0.85
RUF-p900-CO2-1h	0.270	0.296	0.91
RUF-p900-CO2-2h	0.464	0.442	1.05
RUF-p900-CO2-3h	0.491	0.529	0.93

7. Inverse gas chromatography

Inverse gas chromatography at infinite dilution conditions (IGC-ID) measurements were performed with a Fisons Mega HRGC 2 equipped with a two flame ionization detectors [16]. Stainless steel columns with a 2 mm internal diameter, filled with the sample materials, were utilized. The measurement temperature was fixed to 30°C for the RUF resin and to 250°C for the pyrolyzed, and activated carbons. In order to carry out the measurement at infinite dilution, solutes must be injected in small amounts and measured at the limit of detection of the flame ionization detector to find the net retention time. Three injections per solute were executed and the first moments of the gas chromatography peaks were used to compute the retention times. Net retention volume (V_N) can be calculated from the equation, $V_N = Dc \cdot t_N$, where D_C is the flow rate of the carrier gas, helium in this case, and t_N is the measured net retention time. It is possible to relate the free energy of adsorption (ΔG_a) to the net retention volume via $\Delta G_a = -RT \cdot \ln(V_N)$. A linear relation, called an alkane line, is commonly observed when plotting $\Delta G_a(CH_2)$ versus the number of C atoms for a series of n-alkanes. Using $\Delta G_a(CH_2)$, it is possible to determine the surface energy (γ_s^D) via equation (1) [17,18].

$$\gamma_s^D = \frac{1}{4\gamma_{CH_2}} \left(\frac{\Delta G_a(CH_2)}{N \cdot a_{CH_2}} \right)^2 \quad (1)$$

Inverse gas chromatography is an adsorption measurement method in dynamic conditions and used for the characterization of the stationary phase. The measurements were performed at infinite dilution conditions in order to neglect the intermolecular interactions between the injected molecules.

The γ_s^D value is determined from the slope of the straight line obtained from the plot of the n-alkane ΔG_a versus their number of carbon atoms (Figure S5). The straight lines of RUF-p900, RUF-p900-CO2-0.5h, and RUF-p900-CO2-3h are almost superimposed whereas those obtained for RUF-p900-CO2-1h and RUF-p900-CO2-2h are almost parallel to the previous ones, but slightly above. The line corresponding to the RUF resin is clearly different. The value of the slope of the straight lines, $\Delta G_a(CH_2)$, and the corresponding γ_s^D values are reported on Table S3. The surface energy values are around 500 mJ/m^2 for the pyrolyzed, and activated carbons which is ten times higher than that measured for the RUF resin. Such high values are typically measured on graphite or activated carbons [8–11]. Singh *et al.* [9] observed the maximum value for the free energy of adsorption and the surface energy for the sample occurs when the sample was activated in CO_2 for the shortest period of time. Longer activation times lead to a slight decrease of the free energy of adsorption which may be due to the pore widening during activation. These observations are in agreement with our findings: the value of the energy of adsorption and surface energy are the highest for the non-activated carbon and the lowest for the carbon activated for 3 hours in CO_2.

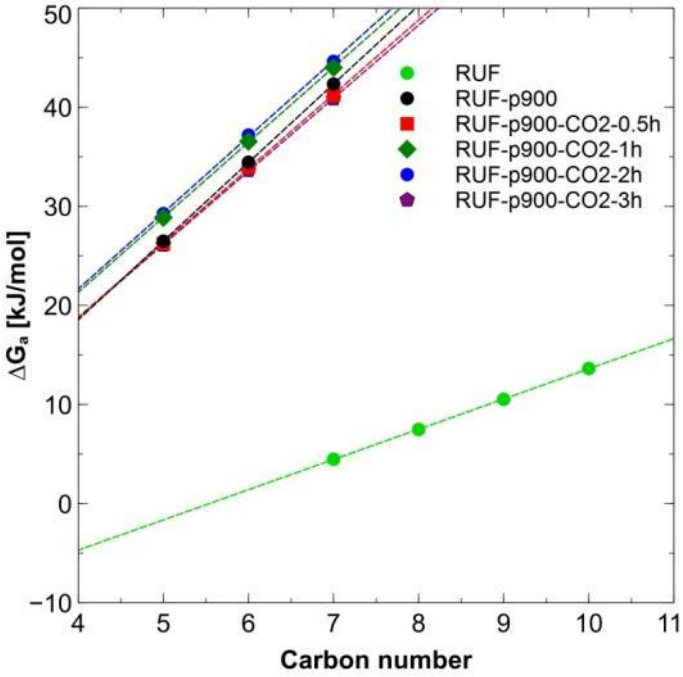

Figure S5. n-alkane straight lines obtained at 30°C for the RUF resin and at 250°C for the pyrolyzed, and activated carbons

Table S3. Results of the slope ($\Delta G_a(CH_2)$) of the n-alkane straight lines and of the corresponding surface energy (γ_s^d) determination at 250°C (except for RUF).

Sample	$\Delta G_a(CH_2)$ [kJ/mol]	γ_s^d [mJ/m^2]	r²
RUF	3.05 ± 0.02	50.9 ± 2.3	1.0000
RUF-p900	7.93 ± 0.02	540.8 ± 23.3	1.0000
RUF-p900-CO2-0.5h	7.49 ± 0.14	483.4 ± 36.7	0.9996
RUF-p900-CO2-1h	7.57 ± 0.07	492.8 ± 27.2	0.9999
RUF-p900-CO2-2h	7.68 ± 0.15	507.3 ± 38.4	0.9996
RUF-p900-CO2-3h	7.37 ± 0.09	467.9 ± 29.1	0.9999

The nanoroughness was determined by comparing the behaviour of the n-alkane probes with those of branched and cyclic probes [12]. The injected probes used for that purpose were: cyclooctane, cycloheptane, and 2,2-dimethylhexane, in the case of RUF and cyclohexane and 2,2-dimethylbutane for the pyrolyzed as well as activated carbons. These molecules are described by their χ_T index. Cyclooctane has a χ_T index of 8.32, cycloheptane, 7.32, cyclohexane, 6.15, 2,2-dimethylbutane, 5.59, and 2,2-dimethylhexane, 7.58.

The morphology index (IM) value is a description of the importance of the size exclusion effects, i.e. of the surface nanoroughness or of the dissolution effects. The values of the morphology index measured during this study are reported in Table S4. An IM value of 1

corresponds to zero size exclusion effect, i.e. flat surfaces at the molecular scale. Lower IM values (for all the probes) indicate stronger size exclusion effects (i.e. nanoroughness).

For the sample RUF, the IM index values determined for the branched and cyclic alkane are close to 0.80. In other words, the surface is only slightly nanorough. The change of nanoroughness from 0.5h to 3h of CO_2 activation is noteworthy. Indeed, the sample activated for 0.5h is strongly nanorough, but with longer activation times, the nanoroughness index of 2,2-dimethylbutane gets close to one which indicates the decreased nanoroughness. The behaviour of the linear and cyclic alkanes is displayed on Figure S6. We observe that, for the sample RUF, the branched and cyclic alkane probes have a similar behaviour like the n-alkanes. In other words, no size exclusion effects are occurring which indicates that the surface is not or only slightly nanorough.

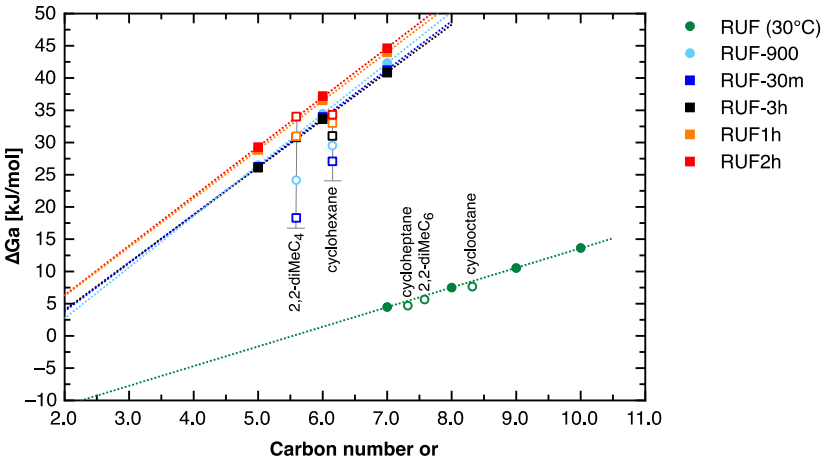

Figure S6. Behaviour of the branched and cyclic alkanes observed at 30°C for the RUF resin and at 250°C for the pyrolyzed, and activated carbons

Table S4. Results of nanoroughness IM index [a.u.] determination at 250°C (30°C for RUF resin).

Sample	2,2-DiMeButane	2,2-DiMeHexane	Cyclohexane	Cycloheptane	Cyclooctane
RUF		0.84 ± 0.03		0.80 ± 0.05	0.75 ± 0.04
RUF-p900	0.19 ± 0.05		0.25 ± 0.01		
RUF-p900-CO2-0.5h	0.05 ± 0.01		0.16 ± 0.01		
RUF-p900-CO2-1h	0.55 ± 0.02		0.34 ± 0.01		
RUF-p900-CO2-2h	0.93 ± 0.04		0.39 ± 0.01		
RUF-p900-CO2-3h	1.00 ± 0.04		0.42 ± 0.01		

The measurements involving the polar probes were also performed at 250°C (30°C for RUF resin). These measurements are carried out using several polar probes: acetonitrile, acetone, THF, ether, chloropentane, isopropanol, dipropylether, dioxane, methyl acetate, benzene, and toluene. Due to the interaction level differences, the same probes could not be measured on RUF. Figure S7 illustrates the behavior of the polar probes as well as the determination method of the specific interaction parameter value ($I_{SP}=\Delta G_a^{sp}$). For each injected polar probe, the obtained I_{SP} values [kJ/mol] are reported in Table S5.

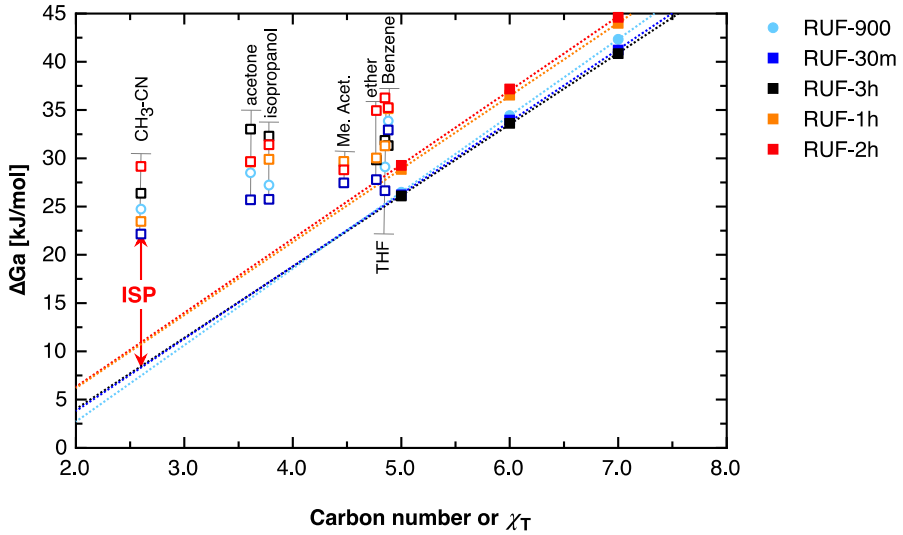

Figure S7 Behavior of the polar probes and I_{SP} value determination at 250°C for the RUF-900, RUF-30m and RUF-3h samples

Table S5 Results of the specific interaction (I_{SP} [kJ/mol]) determination at 250°C (30°C for RUF resin)

I_{SP} [kJ/mol]	**RUF**	**RUF-p900**	**RUF-p900-CO2-0.5h**	**RUF-p900-CO2-1h**	**RUF-p900-CO2-2h**	**RUF-p900-CO2-3h**
Acetonitrile	17.0 ± 0.4	17.3 ± 0.3	13.8 ± 1.1	12.7 ± 0.4	18.2 ± 0.4	17.9 ± 0.3
Acetone	12.5 ± 0.5	13.0 ± 0.5	9.8 ± 1.8	11.2 ± 0.6	11.0 ± 0.5	17.1 ± 0.4
THF	-	3.8 ± 1.0	1.5 ± 0.7	3.5 ± 0.7	8.1 ± 0.7	6.8 ± 1.1
Ether	-	5.3 ± 0.8	3.2 ± 1.0	2.9 ± 0.7	7.4 ± 0.7	5.4 ± 0.7
Chloropentane	5.6 ± 0.3	-	-	-	-	-
i-Propanol	15.7 ± 0.4	10.4 ± 0.7	8.6 ± 0.6	10.2 ± 0.8	11.4 ± 1.1	15.1 ± 0.4
Dipropylether	4.4 ± 0.5	-	-	-	-	-
Dioxane	8.3 ± 0.4	-	-	-	-	-
Methyl Acetate	9.6 ± 0.2	7.0 ± 0.6	5.1 ± 0.6	4.8 ± 0.7	3.5 ± 0.9	-
Benzene	-	8.3 ± 0.6	7.5 ± 1.0	7.2 ± 0.8	6.8 ± 0.7	6.1 ± 0.6
Toluene	5.7± 0.3	-	-	-	-	-
$\sum I_{SP}$ [kJ/mol]	-	58,1 ± 3,9	44,4 ± 6,2	47,7 ± 4,0	62,9 ± 4,1	68,4 ± 3,5

8. Mercury intrusion porosimetry (MIP)

Mercury intrusion was carried out on Pascal 140/440 (Thermo Fisher Scientific Inc.) equipment. The carbon sample RUF-p900-CO2-2h was broken into small pieces with a diameter between 1 and 2 mm and a mass of about 200 mg for the MIP measurement. First, the sample was pre-intruded to 395 kPa (release to atmospheric pressure) in the Pascal 140 and was then moved to the Pascal 440 where intrusion began at atmospheric pressure and increased to a maximum pressure of p_{max} = 200 MPa and then was released (extruded) to atmospheric pressure again. Without removing the sample, a second cycle to p_{max} and release to atmospheric pressure was added [13,14]. In general, raw data from mercury intrusion is analyzed using the Washburn equation [15]. A surface tension of 0.48 N/m^2 and a contact angle of 140° was used in the calculations.

Figure S8a shows the mercury intrusion curves for the sample RUF-p900-CO2-2h. It was found that the pore size distribution is narrow and centered at 8-11 µm (Figure S8b).

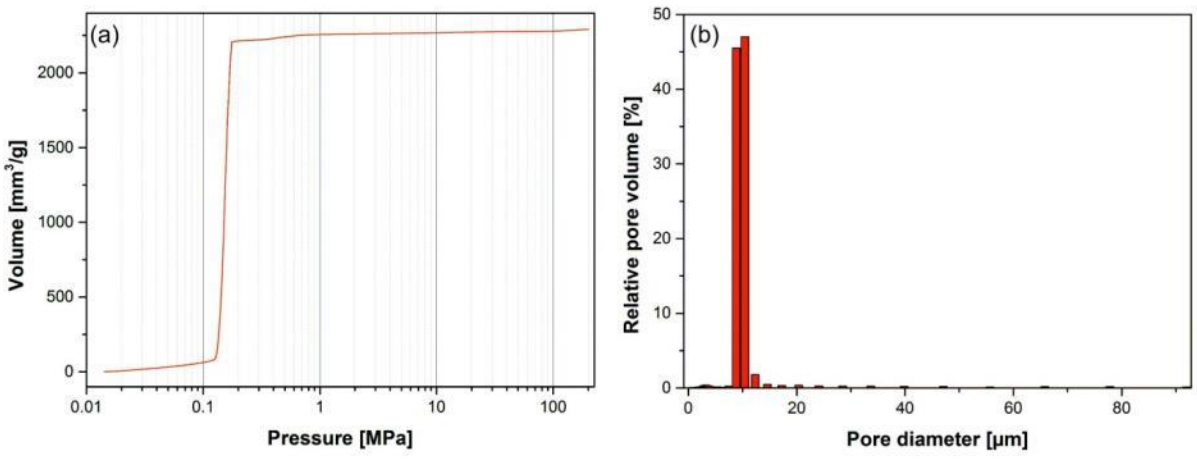

Figure S8 (a) Mercury intrusion curves for porosimetry experiments on sample RUF-p900-CO2-2h and (b) corresponding pore size distribution

9. Elemental chemical analysis (ECA)

Elemental analysis for C, H, and N were carried out by hotgas extraction on a LECO TrueSpec Micro and O analysis with a LECO 628 O Micro instrument. The combustion products of

carbon (CO_2), hydrogen (H_2O), and oxygen (CO) were measured with infrared detectors and N_2 with a katharometer.

Elemental concentrations (C, H, N, O) determined by LECO analysis are shown in Table S6. It can be seen that the atomic concentration of heteroatoms (H, N, O) in the RUF resin is 2 times the concentration of carbon atoms. During pyrolysis at 900°C, the concentration of heteroatoms significantly decreases. However, during physical activation in CO_2, the concentration of hydrogen and oxygen is increased. In general, the concentration of the nitrogen and oxygen functional groups measured by LECO analysis is similar compared to XPS which means that the concentration of heteroatoms in the bulk material is similar to the concentration of those on the surface. In the pyrolyzed, and activated carbons, the concentration of hydrogen is as high as the sum of the concentration of nitrogen and oxygen functional groups.

Table S6 Elemental composition of the dried resin, the pyrolyzed, and the activated carbons

Sample	C [at.%]	H [at.%]	N [at.%]	O [at.%]
RUF	32.76	44.08	8.02	15.14
RUF-p900	78.61	10.76	2.08	8.55
RUF-p900-CO2-0.5h	76.59	11.41	2.29	9.71
RUF-p900-CO2-1h	74.42	13.27	2.07	10.24
RUF-p900-CO2-2h	70.91	14.80	3.18	11.12
RUF-p900-CO2-3h	69.26	15.86	2.64	12.24

10. Water sorption of commercial activated carbons

It is worth mentioning that at a relative pressure below 0.6, the monolith RUF-p900-CO2-3h has a higher water sorption capacity compared to commercial extruded activated carbons which might be due to the higher concentration of surface functional groups of the monolith (Figure S9). Sorbonorit 3 is produced form coconut shell and has reported a specific surface area of ca. 1400 m^2/g whereas Sorbonorit 4 is made from coconut shell and has reported a specific surface area of ca. 1400 m^2/g.

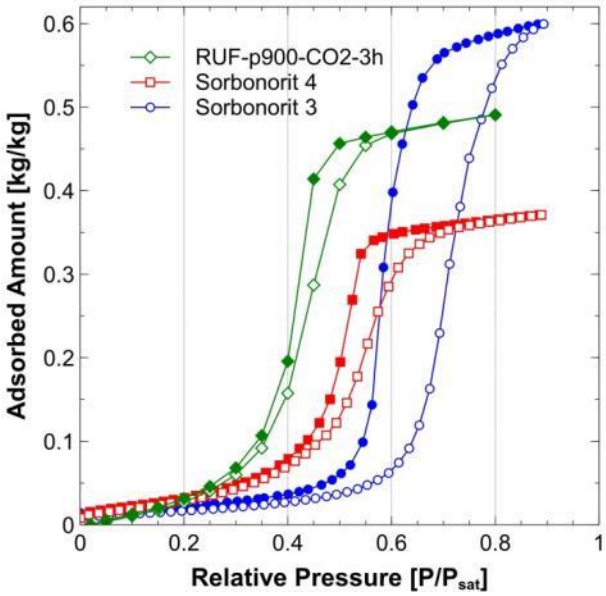

Figure S9 Water sorption isotherms of nitrogen-doped carbon and commercial activated carbons

References

[1] J.R. Pels, F. Kapteijn, J. a. Moulijn, Q. Zhu, K.M. Thomas, Evolution of nitrogen functionalities in carbonaceous materials during pyrolysis, Carbon N. Y. 33 (1995) 1641–1653. doi:10.1016/0008-6223(95)00154-6.

[2] S.R. Kelemen, M.L. Gorbaty, P.J. Kwiatek, Quantification of nitrogen forms in Argonne Premium coals, Energy & Fuels. 8 (1994) 896–906. doi:10.1021/ef00046a013.

[3] E.P. Barrett, L.G. Joyner, P.P. Halenda, The Determination of Pore Volume and Area Distributions in Porous Substances. I. Computations from Nitrogen Isotherms, J. Am. Chem. Soc. 73 (1951) 373–380. doi:10.1021/ja01145a126.

[4] D. Broad, A. Foster, No Title, J. Chem. Soc. 447 (1946).

[5] D.W. McKee, The sorption of hydrocarbon vapors by silica gel, J. Phys. Chem. 63 (1959) 1256–1259. doi:10.1021/j150578a010.

[6] M. Brown, A. Foster, No Title, J. Chem. Soc. 1139 (1951).

[7] L.G. Gurvich, On the physico-chemical force of attraction, J. Phys. Chem. Soc. Russ. (1915) 805–827.

[8] H. Balard, E. Brendle, Carbon black using inverse gas chromatography techniques: Study of the batch to batch stability of the surface properties, KGK. Kautschuk, Gummi, Kunststoffe. (2002) 464–469.

[9] G.S. Singh, D. Lal, V.S. Tripathi, Study of microporosity of active carbon spheres using inverse gas chromatographic and static adsorption techniques, J. Chromatogr. A. 1036 (2004) 189–195. doi:10.1016/j.chroma.2004.03.008.

[10] H. Balard, D. Maafa, A. Santini, J.B. Donnet, Study by inverse gas chromatography of the surface properties of milled graphites, 1199 (2008) 173–180. doi:10.1016/j.chroma.2008.05.012.

[11] F. Lopez-Grazon, M. Pyda, M. Domingo-Garcia, Studies of the Surface Properties of Active Carbons by Inverse Gas Chromatography at Infinite Dilution, Langmuir. (1993) 531–536.

[12] E. Brendlé, E. Papirer, A New Topological Index for Molecular Probes Used in Inverse Gas Chromatography for the Surface Nanorugosity Evaluation, J. Colloid Interface Sci. 194 (1997) 207–16. doi:10.1006/jcis.1997.5104.

[13] J. Kaufmann, Characterization of pore space of cement-based materials by combined mercury and wood's metal intrusion, J. Am. Ceram. Soc. 92 (2009) 209–216. doi:10.1111/j.1551-2916.2008.02834.x.

[14] J. Kaufmann, R. Loser, A. Leemann, Analysis of cement-bonded materials by multi-cycle mercury intrusion and nitrogen sorption, J. Colloid Interface Sci. 336 (2009) 730–737. doi:10.1016/j.jcis.2009.05.029.

[15] E.W. Washburn, Note on a Method of Determining the Distribution of Pore Sizes in a Porous Material, Proc. Natl. Acad. Sci. 7 (1921) 115–116. doi:10.1073/pnas.7.4.115.